Accepted Manuscript

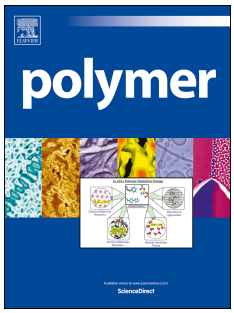

Length controlled kinetics of self-assembly of bidisperse nanotubes/nanorods in polymers

Ali Gooneie, Janak Sapkota, Anuja Shirole, Clemens Holzer

PII: S0032-3861(17)30477-9

DOI: 10.1016/j.polymer.2017.05.010

Reference: JPOL 19670

To appear in: *Polymer*

Received Date: 3 April 2017

Accepted Date: 3 May 2017

Please cite this article as: Gooneie A, Sapkota J, Shirole A, Holzer C, Length controlled kinetics of self-assembly of bidisperse nanotubes/nanorods in polymers, *Polymer* (2017), doi: 10.1016/j.polymer.2017.05.010.

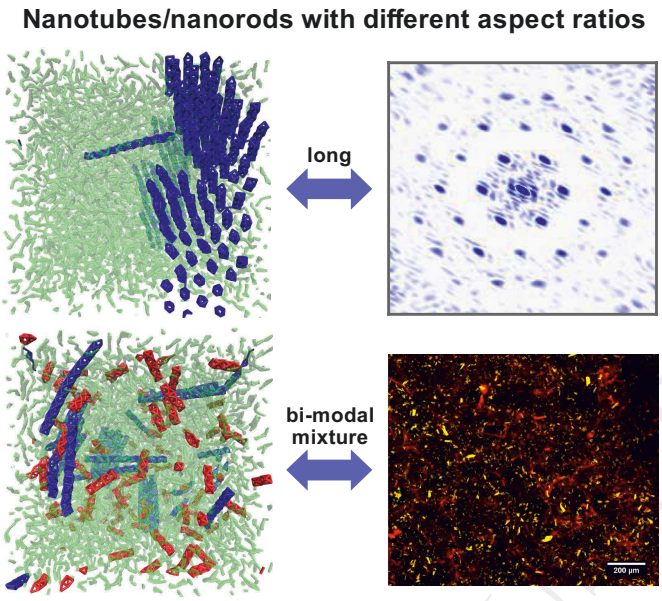

Length Controlled Kinetics of Self-Assembly of Bidisperse Nanotubes/Nanorods in Polymers

Ali Gooneie[1,2,*], Janak Sapkota[1,*], Anuja Shirole[3], Clemens Holzer[1]

[1]Chair of Polymer Processing, Department of Polymer Engineering and Science, Montanuniversitat Leoben, Otto Glöckel-Straße 2, Leoben 8700, Austria. Email: ali.gooneie@unileoben.ac.at, janak.sapkota@unileoben.ac.at.

[2]Laboratory for Advanced Fibers, Empa, Swiss Federal Laboratories for Materials Science and Technology, Lerchenfeldstrasse 5, CH-9014 St. Gallen, Switzerland. Email: ali.gooneie@empa.ch.

[3]Adolphe Merkle Institute, University of Fribourg, Chemin des Verdiers 4, Fribourg 1700, Switzerland.

Abstract.

While there is a growing body of work that supports the self-assemblies of nanotubes and nanorods, little attention has been devoted to understand the relation between their length and the kinetics of self-assembly in polymer composites. Using dissipative particle dynamics (DPD) method, we simulated the temporal developments of equilibrium microstructures of nanotube dispersions with a bimodal length distribution in polymer matrix. The nanotube/polymer models were developed with different sets of interactions between the components. The equilibrium morphologies obtained for nanotubes are in good agreement with those proposed by previous experimental and theoretical studies. We found that long nanotubes could self-assemble into ordered honeycomb-like bundles as validated with the structure factor calculations. The self-assembly kinetics was quantitatively estimated at

different stages and length scales using the variations in the pair-correlation functions. It was observed that the kinetics slowed down particularly in the initial stages of the self-assembly. This was mainly ascribed to the spatial interferences of bidisperse nanotubes as evidenced by laser scanning microscopy and simulated mean-squared-displacements (MSD). Furthermore, the developed microstructures were assessed in terms of the effective nanotube volume derived from Monte Carlo (MC) calculations and the frequency of nanotube-nanotube contacts. The simulations reported herein contribute to a microscopic interpretation of the literature results, and the findings of this paper contribute meaningfully to the design strategies aimed at achieving novel nanocomposites with optimal physical properties.

Keywords: nanotubes, nanorods, bidisperse mixtures, self-assembly, kinetics, nanocomposites, dissipative particle dynamics, cellulose nanocrystals, dispersion

1. Introduction

Nanofillers are attracting a great deal of attention due to their intrinsic characteristics and broad applicability in the areas such as optics [1], electronics [2] and catalysis [3]. Most of the nanofillers used are either spherical or isotropic particles mainly due to the ease of synthesis [4], consequently, leading to isotropic materials. One possible route to the development of the anisotropic structures for mechanical, electrical and optical applications is to use anisotropic nanoparticles such as nanotubes and nanorods [5]. In many cases, a pre-requisite for effective application of nanotubes and nanorods is their stable and homogenous dispersion within the respective matrix due to the fact that agglomeration cancels out most of the benefits of its nano dimensions [6,7]. Therefore, for several other applications, a balance between a stable dispersion and control of the spatial distribution and orientation within the matrix is the key to exploit their outstanding properties on macroscopic scale [8]. The design and preparation of aligned or self-assembled nanotubes/nanorods have been actively researched recently [9]

since the emergence of ordered structures can be used in several practical strategies for designing structural materials [10].

Self-assembly processes which are common in nature are mimicked or utilized as a reference to many dynamic [11] and multicomponent systems [12–14], from smart materials to self-healing structures [15,16] to sensors [17] and spontaneous development of patterned structures [18]. These assemblies are desired due to the modulation of their physical properties [4,19–23] which can be achieved either by equilibrating between aggregated and non-aggregated states of nanofiller [23,24], or adjusting their positions relative to one another in an aggregate [25]. Such spontaneous organization could be directly due to the specific interactions and/or indirectly through their environment. In this context, understanding the phenomena of the nanotube/nanorod self-assembly is essential for materials design; however, it poses many challenges considering the complex thermodynamic and kinetic behavior involved in the assembling process [26–28].

The increase in nanotubes (or nanorods) concentration in the matrix considerably enhances the probability of close tube (or rod) encounters and can eventually block each other's movements to an extent such that no further reorganization is possible [29,30]. Such phenomenon is referred to as rigidity percolation [30], or physical gelation, and is related to the kinetic arrest of the nanotubes/nanorods. For tubular nanoparticles such as carbon nanotubes (CNT), such a kinetic arrest has been experimentally determined to take place starting from the isotropic liquid state at extremely low nanotube volume fraction of ~0.003 [31]. As for the rod-like nanoparticles, the corresponding gelation phenomenon of cellulose nanocrystals (CNCs) typically occurs at higher nanorod concentrations of ~0.08 [30]. However, the length polydispersity and extreme aspect ratio of nanotubes and nanorods have important roles in triggering the transition before any liquid crystalline ordering. The monodisperse colloids of rod-shaped *fd* virus for instance are known to self-assemble in

cholesteric/chiral and sematic phases [32–34] or even in columnar crystal phases [33], whereas high polydispersity (55%) of goethite nanorods can also form such ordered structures [35]. For nanotubes such as CNTs, only nematic phase has been reported thus far, mainly due to the large size distribution of nanotubes and difficulty in preventing particle aggregation [36–39]. This implies that, apparently, for the monodisperse systems it is easier to promote the prevalence of ordered phases [40,41] whereas for high polydispersity the large-scale rearrangements can be constrained by subsequent phase segregation [42]. Bacterial CNCs with an aspect ratio in the range of 50-100 [43,44] also show nematic ordering well below 1 wt% of CNC content [43]. For CNC nanorods which show high polydispersity depending on the source and method of extraction [30,45,46], the influence of the aspect ratio can be recognized as anisotropic phase for longer CNC nanorods [43] and isotropic fractionation of shorter nanorods [47].

With the increasing difficulties in the way of realizing the underlying mechanisms in dispersions of such anisotropic nanoparticles, modelling and simulation techniques have raised tremendous attention [48]. Among various methods, mesoscopic approaches, which define a coarse-grained model of the material, have been extensively used to study the microstructure developments under equilibrium due to their feasibility to access longer time scales [49–55]. Detailed atomistic simulations, on the other hand, have been also applied to characterize the fundamental thermodynamic properties of such dispersions [52,56,57]. While there is a growing body of work that supports the self-assemblies of nanotubes and nanorods, little attention has been devoted to understand their length-controlled assemblies in polymer composites. In order to investigate the length effects, He et al. [58] report the impact of bidisperse nanorod mixtures on their self-assembled morphologies in block copolymers in terms of enthalpy (originated from nanorod-polymer interactions) and entropy (governed by the inherent anisotropy as well as translational entropy of shorter nanorods). However, there is no indication of how the length polydispersity might influence the evolutions of self-

assembled structures with time. This is a relevant question since dissipative particle dynamics (DPD) simulations of Hore and Laradji [59] showed in particular how important it is to consider the length effects of nanorods on the kinetics of phase separation phenomena in immiscible polymer blends.

Here, we present a systematic study of the self-assembly of generalized nanotubes and nanorods with two different aspect ratios, exploring the length effect and the influence of the bimodal length distribution of nanofillers. To do this, we employ the well-credited DPD method to simulate the developments of equilibrium microstructures of such dispersions. We observe that under certain conditions, these nanotubes self-assemble into ordered honeycomb-like bundles. More importantly, the kinetics of this self-assembly was quantitatively described in terms of the variations in the pair-correlation profiles. The results show a reduced self-assembly kinetics particularly in early stages for bidisperse mixtures. Possible correlation of such behavior is also studied with the help of cellulose nanorods where the length induced aggregation/dispersion and its influence on mechanical properties is observed. The detailed understanding of length controlled kinetics of self-assembly for a mixed system with varying aspect ratio of nanotubes, to the best of our knowledge, is the first of its kind. Taken together, the findings of this paper provide a valuable tool that opens innovative ways to implement new routes to design and produce novel composite materials with optimal physical properties.

2. Simulation Details

2.1. Dissipative Particle Dynamics

DPD is a coarse-grained numerical method in which the degrees of freedom of the system are reduced by lumping a number of atoms into the so-called beads [60,61]. These beads interact with each other through three pairwise forces: (i) the conservative force F_{ij}^{C}, (ii) the dissipative

force F_{ij}^{D}, and (iii) the random force F_{ij}^{R}. For any pair of *i* and *j* beads within the force cutoff radius r_c, these forces are given by

$$F_{ij}^{C} = a_{ij}\left(1-\frac{r_{ij}}{r_c}\right)\hat{\mathbf{r}}_{ij}\,, \tag{1}$$

$$F_{ij}^{D} = -\xi_{ij}\omega^{D}(r_{ij})r_{ij}\left[(\mathbf{v}_i-\mathbf{v}_j)\cdot\hat{\mathbf{r}}_{ij}\right]\hat{\mathbf{r}}_{ij}\,, \tag{2}$$

$$F_{ij}^{R} = \sigma_{ij}\omega^{R}(r_{ij})r_{ij}\zeta_{ij}\hat{\mathbf{r}}_{ij}\,. \tag{3}$$

In these equations, r_{ij} is the distance between the beads with the corresponding unit vector of $\hat{\mathbf{r}}_{ij}$ which points from bead *j* to bead *i*. $\mathbf{v}_i$ and $\mathbf{v}_j$ are the velocity vectors of beads *i* and *j*, respectively. The model parameters used in DPD include the maximum repulsion coefficient a_{ij}, the friction coefficient ξ_{ij}, the noise amplitude σ_{ij}, and a Gaussian random number ζ_{ij}. In DPD formulation, $\omega^{D}(r_{ij})$ and $\omega^{R}(r_{ij})$ are the dissipative and random weight functions, respectively, which are often defined as

$$\omega^{D}(r_{ij}) = \left[\omega^{R}(r_{ij})\right]^2 = \left(1-\frac{r_{ij}}{r_c}\right)^2. \tag{4}$$

DPD is an efficient mesoscopic method to study the phenomena on longer time scales than the classical molecular dynamics [62]. This is mainly due to its coarse-grained representation of the system as well as the soft potential functions that it incorporates. For these reasons, DPD has been widely used to investigate multicomponent systems such as polymer/layered silicates [60,63] and polymer/CNTs [49,64]. Here, we employ DPD in order to simulate dispersions of nanotubes in a polymer matrix under thermodynamic equilibrium. In the developed model all parameters are in reduced DPD units unless mentioned otherwise. The selected DPD units are explained later in the context.

2.1.1. Polymer Model

In order to represent a flexible polymer chain, 10 DPD beads were linked by finitely extensible nonlinear elastic (FENE) springs with the potential of

$$U_{FENE}(r_{ij}) = -0.5\, k_s\, r_0^2 \ln\left(1-\left(\frac{r_{ij}}{r_0}\right)^2\right), \quad (5)$$

in which k_s is the FENE spring constant, and r_0 is the maximum extent of the bond. Here these values were set to 50 k_BT/r_c^2 and 0.7 r_c, respectively, which ensures that no unphysical bond crossings are present in the system [65,66]. Each two consecutive bonds were allowed to have any angle in order to preserve the flexibility of the chain.

2.1.2. Nanotube Model

To incorporate a realistic model rather than a generic representation for the nanotubes, we used the model of Liba et al. [67] who developed a coarse-grained model of CNTs by lumping carbon atoms into DPD beads which interact with each other through pair and triplet forces. As shown in Figure 1, each CNT tube is composed of a series of triple-bead rings connected by harmonic bonds with the potential of

$$U_{harmonic}(r_{ij}) = k_h(r_{ij} - r_0)^2, \quad (6)$$

where k_h is the harmonic spring constant. Following Liba et al. [67], k_h was 2675.8 k_BT/r_c^2 and r_0 was 0.6239 r_c. The authors also defined angular forces in order to correctly capture the stiffness of the CNTs. The potential function of these forces is given by

$$U_{angle}(\theta) = k_a(\cos\theta - \cos\theta_0)^2, \quad (7)$$

with k_a, θ, and θ_0 as the angular potential constant, the angle of triplets of neighboring beads, and the equilibrium angle, respectively. In the present model, k_a and θ_0 were set to 38.9 k_BT and 180º, respectively. To model the long nanotubes, 60 beads were included in each tube in the form of 20 triplet rings. For the short nanotubes, on the other hand, 18 beads were used in each tube in 6 triplet rings.

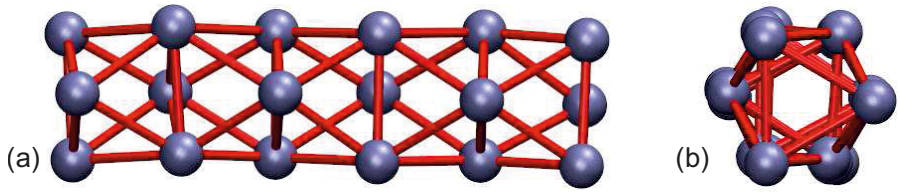

Figure 1. Coarse-grained nanotube structure after equilibration: (a) side view, and (b) cross-sectional view.

The nanotube model with this characteristics also qualifies to be an appropriate representative for a generic nanorod. In order to correctly capture the nanorod, it must be ensured that the inner core of the nanotube is not accessible to the surrounding beads. By taking the geometrical as well as the force field parameters into account, it is possible to rule out any interference of the polymer beads within the nanotubes. We calculate the acting forces on a random bead approaching the nanotube (from the nanotube beads and other polymer beads) and show that it is very unlikely for it to pass through the nanotube in the Supporting Information. A similar approach has also been used before to avoid unphysical bond-crossings in DPD models of polymer chains [66,68]. As a result of such calculations, one can use our simulations to verify nanoparticles resembling nanorod characteristics with a comparable mechanical profile. An example for such nanoparticles is cellulose nanorods which have received a lot of attention recently due to their superior mechanical properties (comparable to CNTs) [69], their bio-compatibility [70], and their relatively lower costs [71]. Because of these reasons, in this paper we also attempt to provide some experimental evidence for cellulose nanorods in order to persuade future works on their mesoscopic simulation. It should be noted that in this paper the term “nanotube” is generally preferred over “nanorod” since it is a more accurate description of the incorporated nanoparticles. Indeed, “nanorod” is also used in several instances where it is investigated.

2.1.3. DPD Units and Model Parameters

A bisphenol A epoxy resin containing 9 repeating units was selected as the matrix polymer with a molecular weight of 2895.5 g/mol and the density of 1 g/cm^3. Each chain was coarse-grained into 10 beads each having a volume of ~480 □^{3} equal to 24 carbon atoms. Each nanotube bead was also taken to represent the same number of carbon atoms following Zhou et al. [64] This choice of coarse-graining degree yields a unit mass m of 4.80×10^{-25} kg for each bead and a length unit r_c of 1.13×10^{-9} m. The energy unit is E = k_BT at T = 298 K. As a consequence of this set of units, the time unit τ is 1.22×10^{-11} s.

In the simulations, the degree of dispersion was controlled by adjusting the maximum repulsion coefficients between different pairs. a_{ii} value was set to 25 k_BT/r_c for all interactions between beads of the same type in the simulations. For interactions between different beads, we used Groot and Warren's approach which relates the excess repulsion parameter to the Flory-Huggins χ_{ij} parameter as [72]

$$a_{ij} \approx \frac{\chi_{ij}}{0.306} + a_{ii}\,, \tag{8}$$

in which χ_{ij} is determined using the solubility parameters δ_i and δ_j of the interacting beads by

$$\chi_{ij} = \frac{V_{ref}\,(\delta_i - \delta_j)^2}{k_BT}\,, \tag{9}$$

with V_{ref} as a reference average bead volume. This reference volume is taken equal to the average bead volume ~480 □^{3}.The solubility parameter of bisphenol A epoxy was determined by molecular dynamics simulations to be 19 $(J/cm^3)^{1/2}$ [64]. For the nanotubes, different solubility parameters are calculated using molecular dynamics for various geometries and model systems. Maiti et al. [73] report a solubility parameter of ~25.9 $(J/cm^3)^{1/2}$ for CNTs having a diameter similar to this study. Other investigations into this parameter have found values between 18 to 26 $(J/cm^3)^{1/2}$ for a wide range of single-walled, double-walled, and

multi-walled CNTs [74]. In our models, we chose two values of 19 and 25.9 $(J/cm^3)^{1/2}$ in order to provide results for this range of CNT types. Consequently, the maximum repulsion coefficients between the polymer-nanotube pair is 25 k_BT/r_c and 43.2 k_BT/r_c, respectively. Indeed, these values should result in different dispersion qualities. Since in the former case all possible pairs experience equal repulsive forces, we refer to it as the system with the neutral dispersive interactions, i.e. system-*n*. In the latter case on the other hand, the repulsive forces between polymer and nanotube beads should promote a poor dispersion quality. Therefore, we refer to this setup as the system with the unfavorable dispersive interactions, i.e. system-*u*. We also simulated a generic system with the a_{ij} values of 32 k_BT/r_c, 10 k_BT/r_c, and 32.8 k_BT/r_c for the polymer-polymer, polymer-nanotube, and nanotube-nanotube pairs, respectively, in order to have a system with a fine dispersion quality for the sake of comparison. This set of repulsion coefficients have been successfully used before to model fine dispersions of layered silicate nanoparticles in compatibilized polymers [63]. This system is referred to as the system with the favorable dispersive interactions in this paper, i.e. system-*f*. The maximum repulsion coefficients of all systems have been summarized in Table 1. In this work, ξ_{ij} was set to 4.5 $(mk_BT/r_c^2)^{1/2}$ between all bead types. Finally, the fluctuation-dissipation theory was used to define the noise amplitude as $\sigma_{ij}^2 = 2\xi_{ij}k_BT$ [75]. In all systems, the force cutoff radius was set to 1 r_c.

Table 1. The maximum repulsion coefficients of different systems.

Pair type	System-*u*	System-*n*	System-*f*
Polymer-polymer	25	25	32
Nanotube-nanotube	25	25	32.8
Polymer-nanotube	43.2	25	10

The simulation box had the dimensions of 22 r_c×22 r_c×22 r_c which represents a cube of real spatial dimensions of 24.86 nm on each side. A total of 32000 beads of different types were dispersed in this box producing a bead number density of 3. The simulated systems contain a nanotube volume fraction of 0.1125 which is equivalent to 3600 nanotube beads out of the total number of beads. Three different systems were developed in order to investigate the impact of nanotube length on the microstructure development: (i) a system containing only short nanotubes with an aspect ratio of 3.5 referred to as the mono-short system, (ii) a system containing only long nanotubes with an aspect ratio of 13.4 referred to as the mono-long system, and (iii) a system containing a 50/50 mixture of such short and long nanotubes referred to as the mixture system. In the mono-short and mono-long systems, 200 and 60 nanotubes were included in the simulation box, respectively. In the mixture system, 100 short and 30 long nanotubes were incorporated.

2.2. Simulation Method

The simulations were carried out in a cubic box with periodic boundary conditions on all sides using NVT ensemble. The systems were constructed with a random dispersion of polymer chains and nanotubes within the box. This configuration was initially allowed to equilibrate for 10^6 steps. Afterwards, the data collection was performed for 2×10^6 steps. The time step was set to 0.01 τ in all simulations. Therefore, the equilibration and data collection runs correspond to the real times of 122 ns and 244 ns, respectively. In addition to these simulations, a separate set of runs were performed on the nanocomposites with a well-dispersed microstructure after altering their force fields to the neutral dispersive interactions. These simulations were run for 10^7 steps corresponding to a real time of 1.22 μs. The simulations were performed using LAMMPS (large-scale atomic/molecular massively parallel simulator) [76] code package. The visualization of the simulated trajectories were carried out in VMD (visual molecular dynamics) [77].

2.3. Investigation of Effective Volume of Nanotubes

The effective volume of nanotubes in the dispersions is defined as the total volume in the simulation box which is within a certain radius of at least one nanotube. In order to quantify the effective volume of nanotubes in the dispersions, we used a Monte Carlo (MC) approach. For this purpose, each nanotube was replaced with a sphere whose center was the center of mass of the nanotube in space. The radii of the spheres were selected to match the corresponding volume fraction of each nanotube in the system. An ideal dispersion of nanotubes was also developed for each system in which these spheres were uniformly dispersed in the simulation box. Such a uniform dispersion should correspond to the largest effective volume due to the minimized overlaps of spheres which occur because of aggregation of nanotubes in any region of the box. To perform the calculation, 10^5 random points were put in the simulation box. If a point was inside any of these spheres, it was considered as a hit. For the simulated and ideal systems, the number of hits were counted and the total number of hits in the simulated systems were divided by the total number of hits in the ideal system to give the dispersion possibility index. This operation was repeated 30 times for each system. In a non-ideal dispersion, the spheres are more concentrated in certain regions of the box and also overlap to some extent. Therefore, a larger dispersion possibility index (with a maximum value of 1 for an ideally-dispersed system) means a better dispersion quality of the system as well as a larger effective volume of the nanotubes.

3. Experimental Details

Tunicate CNCs (tCNC) were isolated using sulfuric acid hydrolysis from the dry mantles of tunicates (Styela clava), and cotton cellulose nanocrystals (cCNC) were obtained via sulfuric acid hydrolysis of filter paper using previously established protocols [6,7,30]. cCNCs and tCNCs were labelled with fluorescein isothiocyanate and rhodamine isothiocyanate (both

obtained from Sigma-Aldrich and used as is), respectively, adapting an earlier protocol [30,78]. Briefly, lyophilized cCNCs or tCNCs (250 mg) were dispersed in dry anhydrous dimethyl sulfoxide (DMSO, 50 mL, Sigma-Aldrich) by stirring the mixture in a round bottom flask overnight at room temperature. The dispersion was then sonicated for 3 h in an ultrasonic bath (45 kHz, 180 W) before adding either fluorescein 5(6)-isothiocyanate (2.5 mg, Sigma-Aldrich) to the cCNC dispersion or rhodamine isothiocyanate (2.5 mg, Sigma-Aldrich) to the tCNC dispersion. Both reaction mixtures were stirred at 90 °C for 6 h, allowed to cool to room temperature, and centrifuged at 3500 rpm for 15 min. The supernatant was decanted, DMSO was added, and the centrifugation and decanting cycle was repeated. This washing/centrifugation cycle was repeated with di-methly formamide (DMF, Sigma-Aldrich) ten times to remove any unreacted dye. The final dispersions were drop cast on the glass slide, at a concentration of 5 mg/mL, evaporated by drying in an oven at 70 °C for 4 h and were studied with laser scanning microscopy using an excitation wavelength of 488 nm for fluorescein and 561 nm for rhodamine to analyze the dispersion and self-assembly behavior.

4. Results and Discussion

4.1. Formation of Self-assembled Microstructures

In order to study the formation of self-assembled microstructures, various mixtures of nanotubes were simulated by altering the nanotube-nanotube, nanotube-polymer, and polymer-polymer interactions. Figure 2 shows the corresponding equilibrium microstructures of the systems. The influence of the dominating interactions on the final microstructure is significant as observed in the resulting trajectories. In the mono-long system, when the interactions among the constituents is changed from a favorable dispersive (system-*f*) to an unfavorable dispersive situation (system-*u*), the microstructure is also altered from a random well-dispersed to a self-assembled state [79]. The same trend is also observed for short

nanotubes, however, with interesting distinctions. Similar influence of the interactions between the nanotubes/nanorods and the matrix on the equilibrium morphology has also been observed before in, for instance, coarse-grained molecular dynamics simulation of dispersed gold nanorods in lipids [80], generic DPD models of nanorods in polymers [81], and hybrid particle-field molecular dynamics simulations of CNTs in different polymers [79]. Moreover, experimental investigations on nanorods dispersed in polymers have also revealed the importance of energetic contributions from nanorod-polymer and nanorod-nanorod interactions in the inter-rod ordering and formation of aligned microdomains [82,82]. The simulations clearly suggest that the small nanotubes do not form a self-assembled microstructure under any circumstances studied. Even for the unfavorable dispersive interactions, the short nanotubes develop small disordered aggregates rather than an ordered self-assembly. In addition to the effective force field, the aspect ratio (or the length in this case) of the nanotubes also shows to be of prominence. The tendency of long nanotubes to go into such assemblies is much higher than the short nanotube. This can be readily seen in system-*n* where the equilibrium microstructure is controlled by the shape of the particles rather than the interactions between the components (see parts c and g in Figure 2).

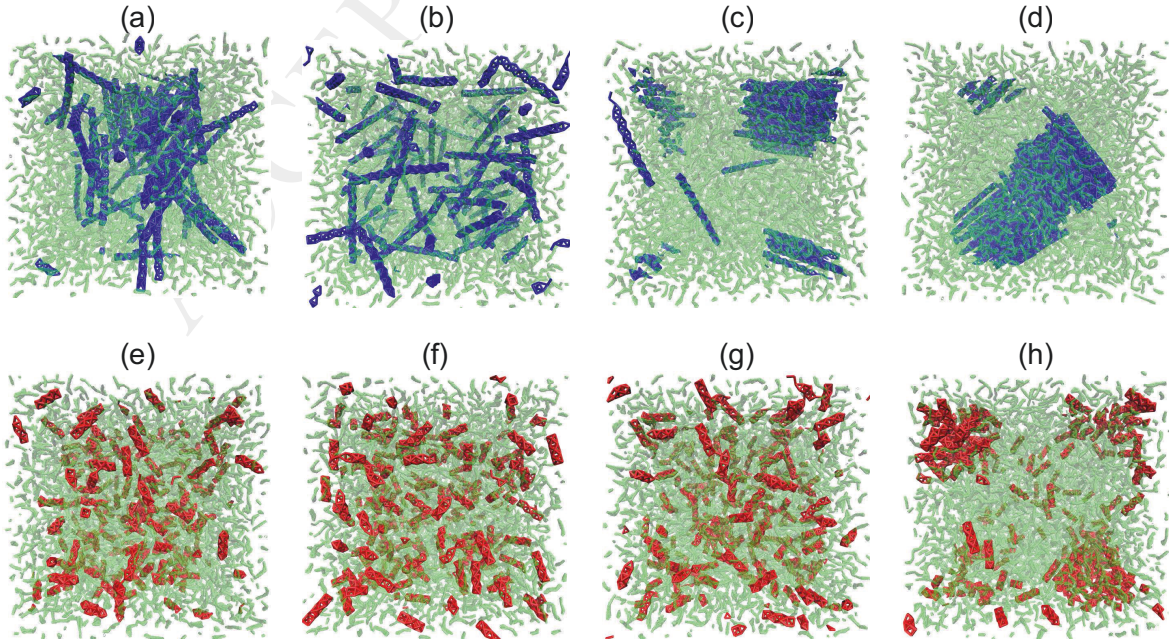

Figure 2. The equilibrium microstructures of nanotubes in polymer for long (a to d) and short (e to h) nanotubes: (a, e) the initial microstructure, (b, f) system-*f*, (c, g) system-*n*, and (d, h) system-*u*. The long and short nanotubes are shown in blue and red, respectively. The polymers are presented in green in all parts.

To visualize the ordering of nanotubes in the self-assemblies of long nanotubes in equilibrium, the two dimensional structure factor of the beads S(***k***) in a bundle was evaluated on a plane perpendicular to the bundle using the relation [83]

$$S(\mathbf{k}) = \frac{1}{N}\langle\left[\sum_{i=1}^{N}\cos(\mathbf{k}\cdot\mathbf{r}_i)\right]^2 - \left[\sum_{i=1}^{N}\sin(\mathbf{k}\cdot\mathbf{r}_i)\right]^2\rangle\,, \tag{10}$$

in which N is the total number of beads in the bundle, with position vectors **r**. The resulting structure factor is shown in Figure 3a. The long nanotubes are packed in such bundles and form a honeycomb pattern as evidenced by the structure factor. A similar honeycomb structure was also reported before in simulations of polymer-tethered nanorods [50] and bidisperse nanorods in block copolymers [58], and experimentally for alkane-covered CdSe nanorods in poly(methyl methaacrylate) [84], and CdSe nanorods in copolymer-based supramolecules [82], and carbon nanotube bundles [85]. It was argued that these structures are formed due to the interplay between liquid crystal ordering and microphase separation based on Brownian dynamics simulations. This ordering is observed in all of the self-assembled bundles of long nanotubes while an irregular aggregation dominates the short nanotubes. The periodic regularity in the assemblies is extended when the number of participating nanotubes is larger in that assembly. The distancing of nanotubes from each other is, however, constant in different assemblies and depends on the excluded volume considerations due to the conservative forces [81,86]. The pair correlation function g(r) of nanotube beads were calculated for the long nanotubes in system-*u*, see Figure 3b. In the calculations of g(r) throughout this paper, the correlation of each bead is measured only with beads from other nanotubes. This enabled us to remove the contributions of the bonded beads as well as other beads within the same nanotube from g(r) and hence provide a more accurate evaluation of the self-assembly. The g(r) profile shown in Figure 3b corresponds to the equilibrium

microstructure developed in Figure 2d. As shown in this profile, the beads do not cross each other and a minimum distance of ~0.6 r_c exists between each pair of beads due to the strong conservative forces between these beads. Moreover, a notable maximum in the data is observed at ~1.5 r_c which can be ascribed to the self-assembled structures within the bundles. This distance represents the average distance between the outer layer of beads on the surfaces of two adjacent nanotubes in a bundle describing the periodicity length observed in the structure factor pattern. Since this maximum distinguishes between the regular assembled structures versus the irregular dispersions, the value of g(r) at this separation distance can be taken as a reference point for comparison between different microstructures. Recently, a similar trend was also observed in generic DPD models of nanorods in a polymer matrix in which the alignments of neighboring nanorods in the bundle and the periodicity in the structure were characterized in terms of the first peak in g(r) profile [81].

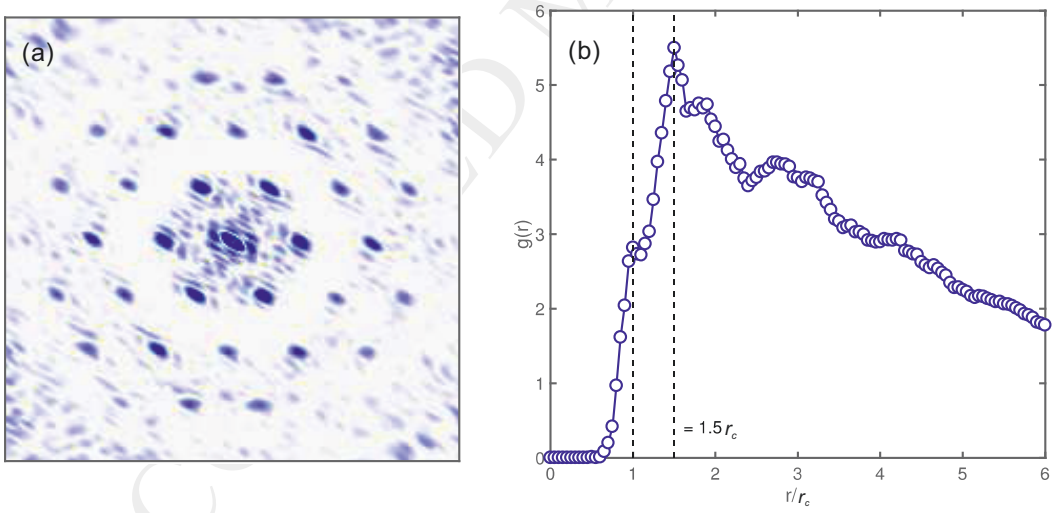

Figure 3. (a) 2D-structure factor of a self-assembled bundle of long nanotubes projected onto its normal cutting plane in system-*u*. (b) Pair correlation function g(r) of the nanotube-nanotube beads for the long nanotubes in system-*u*.

An influencing parameter on the self-assembly of nanotubes is the length of the nanotubes as evidenced by the system trajectories in Figure 2. As noted before, the long nanotubes tend to form ordered assemblies while the short ones hardly undergo the aggregation process, and even when they do, the resulting structures are irregular. An interesting case is when a

mixture of such short and long nanotubes are allowed to equilibrate together. Recently, the importance of such mixtures were investigated by Sapkota et al. [30] for crystalline cellulose nanorods where the mechanical properties showed significant dependence on the dispersion mechanism. Some other studies have also shown the advantage of mixing geometrically different fillers to enhance filler dispersion and subsequently enhance mechanical, electrical or thermal properties [87–89]. On the other hand, both nanotube and nanorod samples often have a certain amount of length polydispersity which makes it of more practical relevance to study such mixtures. Here, we simulated a 50/50 mixture (by volume) of long and short nanotubes to find the underlying mechanisms involved in their microstructure developments. The simulated microstructures are shown in Figure 4(a-d). A comparison of the equilibrium structures in the mixtures with the structures of the mono-length systems suggests that, apparently, the short and long nanotubes equilibrate separately and each phase (the long nanotubes phase, and the short nanotubes phase) reaches its equilibrium microstructure very much the same as their corresponding mono-length systems. However, some interference from the short nanotubes can already be seen in the trajectories where the short ones appear to have been incorporated between the self-assembled structures of the long nanotubes. To investigate this possibility, the average mean-squared-displacements (MSD) of the centers of mass of the nanotubes were calculated according to $\mathrm{MSD} = \langle [\mathbf{r}_i(t) - \mathbf{r}_i(0)]^2 \rangle$ with $\mathbf{r}_i(t)$ and $\mathbf{r}_i(0)$ representing the position vectors of the center of mass of the *i*th nanotube at the start of the simulation and at time t, respectively [60]. In the mixture system, the MSD of short and long nanotubes were calculated separately so that a better perspective of their relative differences with the mono systems can be envisioned. The results of such calculations are plotted in Figure 4 for system-*u* (part e) and system-*f* (part f). In the mono systems, the short nanotubes show much larger displacements in comparison with the long ones regardless of the effective pair interactions. Indeed, the long nanotubes face stronger topological restrictions against their movements due to their larger surface area [90]. Moreover, they self-assemble

and form bundles which makes it even more difficult for the bulky bundles to move in the simulation box. The short nanotubes, on the other hand, can adopt more random patterns in their movements and transport faster on larger length scales. They preserve their individuality to a large extent even in system-*u* with unfavorable dispersive interactions where dispersed irregular aggregates are formed instead of a tightly-packed self-assembled bundle. In the mixture of short and long nanotubes, the displacement patterns of the nanotubes is very close to the mono-long system regardless of their length. The interesting observation that the short nanotubes in the mixture move almost as slow as the long nanotubes supports the earlier statement that the short nanotubes interfere with the self-assembly of the long nanotubes. Thus, the microstructure development is not merely followed by one nanotube phase independently from the other phase. Therefore, the length of the nanotubes influences the development of equilibrium microstructures significantly in such dispersions.

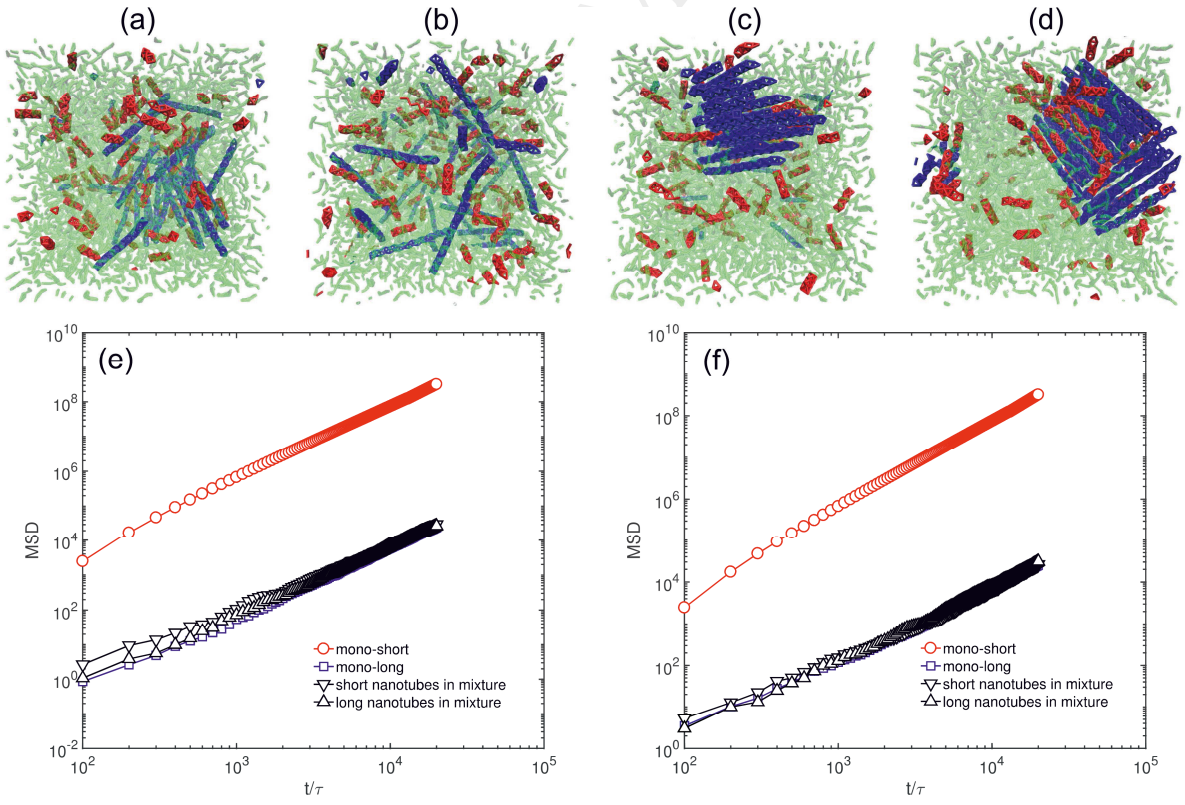

Figure 4. (a-d) The equilibrium microstructures of nanotubes in polymer for the mixture of long (shown in blue) and short (shown in red) nanotubes: (a) the initial microstructure, (b) system-*f*, (c) system-*n*, and (d) system-*u*. The polymers are presented in green in all parts. The

average mean-squared-displacements (MSD) of the center of mass of nanotubes is plotted against simulation time for (e) system-*u* and (f) system-*f*. The movements of the short and long nanotubes in the mixtures are evaluated separately.

The interference of the short nanotubes with the self-assembly of the long nanotubes should particularly influence the kinetics of aggregation. This notion could be engineered in order to develop desired microstructures in such dispersions optimizing their properties. An example could be given by studying the developed microstructures in the dispersions of crystalline cellulose nanorods. Considering the strong topological restrictions against the penetration of any bead into the inner core of the nanotubes as a result of their design and the employed force field [68], it was argued to be reasonable to assume that the nanotubes of this study can also represent a nanorod (see the Supporting Information). In particular, CNC nanorods show comparable mechanical properties to CNTs [69] which were the basis for the developed coarse-grained nanotube models in the work of Liba et al. [67] Consequently, the developed nanotube models can provide, at least, a reasonable generic representation of CNC nanorods. Due to the increasing interest in the development and applications of bio-based cellulose nanocomposites, we provide here laser microscopy evidence for the dispersion of short, long, and mixtures of these two types of CNC nanorods. Figure 5 shows the different aggregation behavior for different aspect ratios of CNC nanorods. The short cCNC nanorods, show a homogenously aggregated structure, with denser agglomerates distributed evenly throughout the macro phase in the nanocomposite. This could be due to the isotropic fractionation of shorter nanorods [47] as previously observed in the simulations. The long tCNC nanorods, show some packed structures resembling self-assemblies and some randomly dispersed pattern. This could be possibly because of the higher aspect ratio which facilitates kinetic trapping and anisotropic phase fractionation [43] in comparison to the short ones. In addition, the tendency of nanorods to orient themselves in parallel to each other and cluster into assembled structures also results from higher lateral capillary forces along the length of a nanorod in comparison to its width [91]. This anisotropy of interaction between nanorods

could be one important driving force for the side by side alignment of nanorods rather than end to end, as also observed in simulations in Figure 2d for instance. The proportion of smaller or larger ordered domains could be controlled by a balance between hydrodynamic and lateral capillary forces [91]. Interestingly, the mixture system shows the kinetic trapping of short nanotubes within the long nanotubes, and a hindered self-assembled structure. Figure 5c shows the colocalized cCNCs within tCNCs as seen with the overlapped spectrums of co-excited rhodamine-labelled tCNCs and fluorescein-labelled cCNCs. Since both the fluorophores are excited at the same time, instead of seeing a green or red dominant region which suggests a clear phase separation, a homogenously co-localized region is observed. The yellow color shows the dominant cCNCs region with tCNCs co-localized in the region, whereas orange color shows clearly tCNCs dominant region with cCNCs co-localized in the region. Furthermore, some parts appear with more reddish color suggesting the assembled tCNCs region. These findings are supported by the recent experimental and modelling studies which suggest a mixed percolating structure and reduced aggregation of short nanotubes in mixtures [30]. Such a co-localization supports the simulation results which show the interferences of the short nanotubes/nanorods within the self-assemblies of the long particles during the microstructure development.

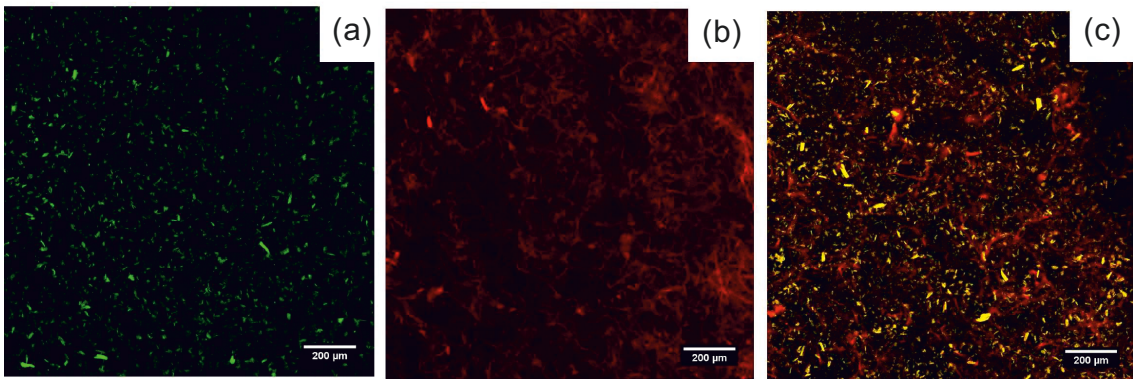

Figure 5. Confocal optical microscopy images of nanocomposites containing 10% w/w of (a) fluorescein-labelled cCNCs (excited at 488 nm), (b) rhodamine-labelled tCNCs (excited at 561 nm), and (c) a 1:1 mixture of these CNC types excited at both wavelengths. Scale bar corresponds to 200µm.

4.2. Controlled Kinetics of Self-assembly

The simulations of the development of equilibrium structures in mixtures of short and long nanotubes indicate the tendency of short nanotubes to incorporate with the self-assembly of the long nanotubes. This interference should influence the kinetics of self-assembly due to the different mobilities of the nanotubes. In order to study such effects, the well-dispersed mono and mixture systems (Figure 2(b, f) and Figure 4b) were simulated to reach a new equilibrium by altering their force field from a favorable dispersive to a neutral dispersive type. Since the repulsive forces between all pairs are the same in the neutral dispersive systems, the length of the incorporated nanotubes is the only playing factor determining the final microstructure. Furthermore, one can minimize the effects of the spatial starting configuration on the final structure by this approach because all systems had already reached an equilibrated well-dispersed dispersion with a steady potential energy from the previous run.

The MSD data were calculated for various systems and are shown in Figure 6. The MSD profiles further support the previous conclusions that the movements of the short nanotubes in the mixtures are significantly hindered by the long nanotubes. Hence, the self-assembly process in such dispersions must be changed due to the interferences of the short nanotubes as well. To investigate the microstructural evolutions during the simulations, we set three intermediate control times t_1 to t_3 in addition to the first and last measurement times t_i and t_f, respectively. The corresponding microstructures at each time are shown in Figure 7 for the mono-long and mixture systems. The mono-short system was almost well-dispersed during the entire run as expected from Figure 2g and consequently was not repeated here. A comparison between the trajectories of the systems during the structure evolution indicates a relatively slower self-assembly kinetics in the mixture system in comparison with the mono-long system. At t_1, the mono-long system has already initiated the self-assembly process and some of the long nanotubes are packed together in the assemblies of a few nanotubes. On the

contrary, the long nanotubes in the mixture do not show any sign of self-assembly yet. The initiated self-assemblies of long nanotubes grow larger as the time proceeds in t_2 and t_3 in the mono-long system whereas their growth is relatively slower in the mixture system. The slower initiation and growth of the bundles is ascribed to the increasing difficulty for the long nanotubes to move in the box and attach to each other in the presence of freely moving small nanotubes. It should be noted at this point that the structure of the self-assembled bundles follows the honeycomb structure (Figure 3a) at all stages of the development as it was shown before by the structure factor analysis. This ordering of long nanotubes prevails in both mono-long and mixture systems.

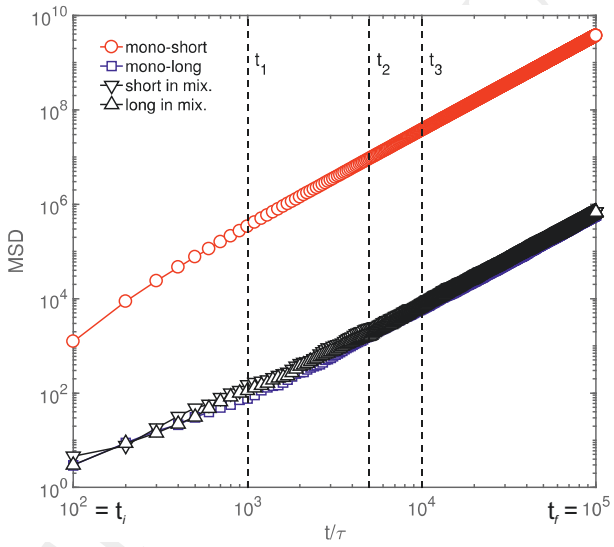

Figure 6. The average MSD of the center of mass of nanotubes against simulation time for system-*n*.

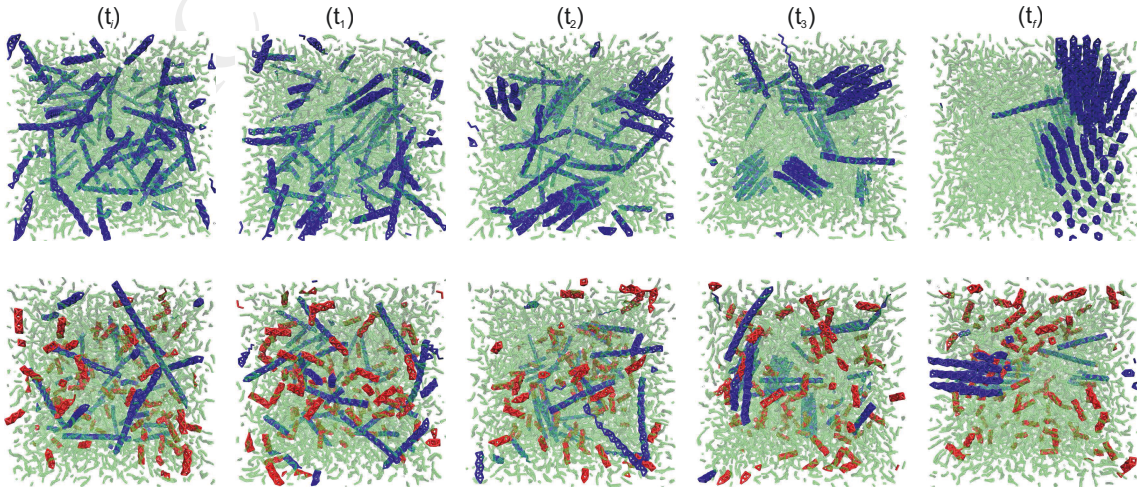

Figure 7. The evolution of microstructure and formation of self-assembled bundles at control times as described in the text. The corresponding time of each column is above it. The first and second rows show the simulated trajectories of the mono-long and mixture systems, respectively. The short and long nanotubes are demonstrated in red and blue, respectively.

The kinetics of self-assembly can be quantified by the development of pair-correlation profiles during the process. Since only the long nanotubes contribute to the self-assembly of ordered bundles, the pair-correlation function of the mixture system was only evaluated for these nanotubes. The kinetics of self-assembly $K_{self\text{-}assembly}$ was monitored by defining

$$K_{self\text{-}assembly} \cong \frac{\delta[g(r)]}{\delta t} = \frac{g(r)|_{t_{k+1}} - g(r)|_{t_k}}{t_{k+1} - t_k}, \quad (11)$$

which is an approximation of the development of g(r) at all r values between two sequential control times t_k and t_{k+1}. $K_{self\text{-}assembly}$ was calculated for transitions between all control times and is shown in Figure 8 for the mono-long system and the long nanotubes in the mixture system. In the early stage of the self-assembly between t_i and t_1, the nanotubes in the mono system start forming the ordered bundles faster than in the mixture. This self-assembly mainly dominates the small length scales, i.e. the nanotubes close to each other come together, as the there is a distinct maximum at ~1.5 r_c. This length scale is in agreement with the periodicity of the honeycomb structure observed in the structure factor patterns (Figure 3a). Since no pronounced assembly is observed at larger r values, one can conclude that the long range patterns have not started to develop yet. In the mixture, on the other hand, the kinetics is much slower than in the mono system particularly at small length scales. These explanations are in agreement with the trajectories of the systems demonstrated in Figure 7 (see control time t_1). As the simulation proceeds in times t_2 and t_3, the self-assembly begins to extend onto larger length scales. Consequently, the kinetics profile shows a faster growth process than previous stage at larger r values up to separation distances ~6 r_c while the self-assembly still proceeds quite fast on short scales as well. This observation suggests the addition of individual nanotubes to the ordered bundles, or the coalescence of small bundles with each other at the intermediate stages of self-assembly. During these stages, the long nanotubes in the mixture

continue to assemble at an almost constant rate at all length scales which is relatively slower than the mono system. At the final stage of the equilibration between t_4 and t_f, the self-assembly rate is almost identical for the long nanotubes in both mono and mixture systems. The long range assembly becomes more pronounced in comparison with the short range assembly. However, it should be noted that the overall kinetics is slowed down by an order of magnitude compared to the intermediate assembly stages. This is mainly because the bundles growth is completed for the most part in the intermediate stages making it a reasonable outcome that the kinetics is slowed down significantly.

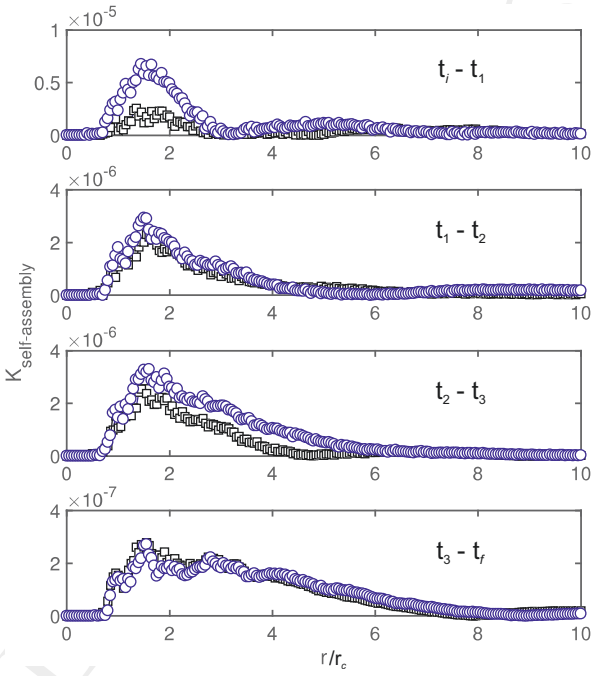

Figure 8. The kinetics of self-assembly $K_{self\text{-}assembly}$ of long nanotubes in the mono-long system (shown in blue circles) and the long nanotubes in the mixture system (shown in black squares). Each part was calculated for two sequential control times as indicated on the corresponding plot.

The variations in the kinetics of self-assembly during different stages of equilibration show a relatively slower rate of assembly of long nanotubes when they are mixed with short nanotubes. This difference is particularly of importance in the early stages of self-assembly when the initial bundles are formed. Furthermore, the addition of farther located nanotubes to these bundles, i.e. the long range assembly, is critically more difficult in a mixture including

highly-mobile short nanotubes. These observations become of practical importance where sonicated dispersions of nanotubes (or nanorods) in a solvent or a low molecular weight polymer matrix are to be developed for further study by, for instance, microscopy techniques. If a mixture of short and long nanotubes is dispersed in a solvent, there is more time to evaporate the solvent and freeze the well-dispersed microstructure before the self-assembly starts to dominate the dispersion. In other words, for a dispersion of long nanotubes in a solvent, ordered bundles develop and start to extend to longer length scales much faster than a mixture of nanotubes with different lengths as the solvent is being removed. Recently, Javita et al. [92] studied the self-assembly of cellulose nanorods in a shrinking droplet experimentally where the solvent was removed at different evaporation rates. Their results were also the same as here that the nematic domains were observed at longer lengths scales as the solvent was removed more slowly. Dumanli et al. [93] also showed that during water evaporation, CNCs in solution progressively assembles into ordered chiral structure on top of the substrate. Indeed, the final microstructure at different length scales is directly linked to the observed material properties. This issue is discussed in the next section.

4.3. Assessment of the Self-assembled Microstructures

A determining factor in how much the nanotubes can improve the mechanical properties of the dispersions is indeed the amount of volume of the matrix which is affected by their presence. In simple words, almost no improvement in the mechanical properties is witnessed if the nanotubes are strongly aggregated together and do not dominate the matrix volume by forming networks with each other as well as with the matrix chains. Therefore, it is also essential to provide insights into the amount of the effective volume in different systems studied. One way to quantify this volume is by the dispersion possibility index. This index varies between 0 and 1 indicating the reverse statistical probability of finding a random spatial point in the box which is not within the effective volume of a random nanotube. Therefore, a

higher amount of effective volume of nanotubes, and consequently a higher reinforcement degree, is reached with an increase in this index.

The evaluated values of the dispersion possibility index are given in Table 2. In system-*u* and system-*n*, the nanotubes in the mono-short and mixture systems influence almost the entire volume of the box effectively. The mono-long system, however, does not influence but only half of the available volume as a result of the self-assembled microstructures. In all systems, the index increases as the unfavorable dispersive interactions are replaced with the neutral and favorable interactions exhibiting an improvement in the effective volume of nanotubes due to better dispersion quality. This trend is more pronounced in mono-long system as the self-assembly process was observed to be strongly dependent on the force field interactions. Even though the long nanotubes in the mixture still assemble in bundles (with a slower rate than mono-long systems) and the short nanotubes are almost ideally dispersed in the box (see Figure 4c), its dispersion possibility index suggests an ideal dispersion quality. This should be a result of (i) the high amount of nanotubes incorporated in the simulation box, and (ii) the high amount of small nanotubes in the mixture. Consequently, one should interpret the dispersion possibility index data considering the microstructures shown before. Still, this index can provide a meaningful statistical measure of the effective volume of nanotubes as incorporated in this discussion.

Table 2. The average dispersion possibility index calculated using MC method.

Type of system	System-*u*	System-*n*	System-*f*
Mono-short	0.927 ± 0.0027	0.979 ± 0.0049	0.986 ± 0.0038
Mono-long	0.495 ± 0.0020	0.523 ± 0.0027	0.971 ± 0.0024
Mixture	0.948 ± 0.0080	0.980 ± 0.0048	0.976 ± 0.0064

The amount of effective volume of dispersed nanotubes/nanorods in a nanocomposite system can be correlated with the percolation concept, which takes into account the interactions between the nanoparticles within the system [30]. Above a certain volume fraction of nanotubes, the nanotubes can only interact with each other in an effective way forming a percolating network. However, in response to the dispersion behavior of nanotubes in composites, only a portion ϕ of the total volume fraction X_r of nanoparticles contributes to the formation of the percolating network. This can be expressed in the following equation [30]

$$\phi = \begin{cases} 0 & :X_r<\psi_c \\ \pi R^2 \rho \left[f_\alpha \int_0^\infty L f_{N_\alpha} \left(\frac{X_r - \psi_c(L)}{1 - \psi_c(L)} \right)^b dL + f_\beta \int_0^\infty L f_{N_\beta} \left(\frac{X_r - \psi_c(L)}{1 - \psi_c(L)} \right)^b dL \right] & :X_r>\psi_c \end{cases} \quad (12)$$

where, $f_\alpha + f_\beta = 1$ corresponding to the volume fraction of α and β filler, A_α and A_β are the aspect ratios of the α and β nanotube, f_{N_α} and f_{N_β} are the length distribution functions of the α and β nanotube, and $\psi_c(L)$ is the percolation threshold of the particle with a length of L, and b is the percolation exponent of power law equal to 0.4 for 3D systems, and ρ is the filler density.

The effective volume fraction is crucial in determining mechanical and physical properties, such as the elastic modulus, or the electric conductivity. Additionally, the presence of an interacting percolation network at a percolation threshold is clearly dominated by the length of nanotubes/nanorods. Based on the new insights from our simulations as well as previous experiments, one can conclude that the percolation threshold of nanotubes/nanorods in the mono-short system is much higher (e.g. empirically ~5 wt% for CNCs [7,30]) compared to the mono-long system (e.g. empirically ~0.8 wt % for CNCs [6,30]). This can be correlated inversely with the dispersion possibility index (see Table 2) and the length of nanotubes/nanorods. In the mixture system, short nanotubes co-localize together with long nanotubes (Figure 5c). As discussed earlier, in the mixture system the short nanotubes are

almost ideally dispersed and even if the long nanotubes assemble in some bundles, the dispersion possibility index would be high since the short ones are bridging the percolation network of the long nanotubes. This is supported by the experimental results with the mechanical reinforcing ability of nanotubes, the use of the combination of nanorods with different lengths resulted in composite materials with similar properties to those of materials containing only well-dispersed long nanorods [30].

The average number of total nonbonded nanotube-nanotube bead contacts are calculated and are given in Table 3. In this work, two beads are in contact if they have a separation distance equal or less than the force cutoff radius. Except for system-*f*, it is clear that the number of contacts are higher in the mono-long system in comparison with the mono-short and mixture systems. This is due to the aggregates that are formed by the long nanotubes leading to the local ordering of the long nanotubes which yields a high possibility for bead-bead contacts. As the quality of dispersions is improved, all nanotubes are almost ideally dispersed in the box. Consequently, the probability of a contact between two nonbonded beads is directly related to the probability of two nanotubes contacting with each other during their movements. This phenomena is manifested in the higher number of contacts in the mono-short system with the highly-mobile nanotubes rather than in the mono-long system with the nanotubes restricted with their movements. In all cases, the mixture has an average value of the mono-short and mono-long systems due to the similar contributions of each phase to the overall number of contacts. As for the electrical properties, it should be noted that the nanotube-nanotube contacts are crucial in order to transport the electrons between nanotubes throughout the material. However, the electrical conductivity also necessitates the formation of a nanotube network throughout the box for the continuous transport of the electrical charges from side to side [79]. As a result, the self-assembled microstructure cannot yield high electrical conductivity unless it forms a continuous structure throughout the entire bulk, for instance, from side to side in a thin film [19]. Such a thin film can be produced for

example by benefiting from geometric confinements in the supramolecular framework [94]. An optimized system for efficient conductivity could be developed by considering the effective volume (Table 2) and the number of nanotube-nanotube contacts (Table 3) simultaneously. In this case, the mixture of short and long nanotubes rather than the mono-length nanotube systems provides the optimum property profile for efficient conductivity particularly if the self-assembly of long nanotubes is frozen before completion. Recent studies on the dependence of the electrical percolation and conductivity of CNTs show that an increase in their aspect ratio or a decrease in the degree of anisotropy in their dispersion significantly alters the percolation probability [95]. This can be correlated with the state of dispersion and/or self-assembly of the nanotubes within the system. The perfectly aligned nanotubes, as in mono-long system, yields a higher drain current only when the tube lengths exceed the channel length, whereas the short CNTs require a formation of the percolation network. In this case, the random dispersion of the mixed system with occasional assembled structure could be an optimal formulation to obtain better electrical conductivity. It was found experimentally that the electrical conductivity was increased when the CNT-containing polyolefinic composites were melt-compounded [96], resulting in reduction in the CNT length during the compounding and better dispersion in such systems with diverse length distribution of CNTs.

Table 3. The average number of nanotube-nanotube contacts.

Type of system	System-*u*	System-*n*	System-*f*
Mono-short	3625	961	214
Mono-long	5955	5712	107
Mixture	4658	2630	161

5. Conclusions

The influence of the aspect ratio of anisotropic nanotube/nanorod dispersions in a polymer matrix on the development of equilibrium microstructures was investigated in this study utilizing coarse-grained DPD models. The results indicated the higher tendency of the long nanotubes to form self-assembled bundles compared with the short nanotubes. The dispersion of high aspect ratio nanotubes resulted in ordered assemblies with a preserved honeycomb packing according to the structure factor calculations. This ordered structures were observed when the dispersive interactions were of a neutral or unfavorable nature while it was absent in the systems with the generic favorable dispersive interactions. For the dispersion of the low aspect ratio nanotubes, a randomly dispersed microstructure was dominant. In such dispersions, the nanotubes formed randomly-structured aggregates rather than ordered bundles even with the unfavorable dispersive interactions.

From the simulations of mixtures of short and long nanotubes, it was evidenced that the short nanotubes interfere with the self-assembly process of long nanotubes. This was firstly deducted from the MSD profiles of the systems. Secondly, laser scanning microscopy of nanocomposites with CNC dispersions supported this realization empirically, thus, proving an altered self-assembly process of long nanotubes in the presence of the short nanotubes. The kinetics of self-assembly was studied in simulations of mono-long and mixture systems with neutral dispersive interactions to highlight the length distribution effects. The results clearly showed a slower self-assembly kinetics in the mixtures which was ascribed to the previously observed interferences of the short nanotubes. The self-assembly kinetics was monitored by calculating the variations in the pair correlation function at different separation lengths. It was observed that the initial stage of the self-assembly, i.e. the formation of small bundles from a few nanotubes, is particularly slower in the mixtures. Moreover, the growth of the bundles on

the larger length scales in the intermediate stages was also manifested to be slower in the mixture system.

We finished the discussion by evaluating the final microstructures using the effective volume from MC calculations, and the number of nanotube-nanotube contacts. These parameters were linked to the mechanical and electrical properties of the final nanocomposites and showed to be in good agreement with previous experiments. In sum, the mixture system was shown to be the viable candidate to show an optimum property profile.

6. Acknowledgements

J. Sapkota and A. Shirole gratefully acknowledge financial support for the experimental work from the Swiss National Science Foundation (NRP66: Resource Wood, Nr. 406640_136911/1) and the Adolphe Merkle Foundation. The authors also thankfully acknowledge Prof. Christoph Weder (Adolphe Merkle Institute) for his support and scientific expertise.

7. References

[1] S.V. Ahir, E.M. Terentjev, Photomechanical actuation in polymer-nanotube composites, Nature materials 4 (2005) 491–495.

[2] B. Pradhan, K. Setyowati, H. Liu, D.H. Waldeck, J. Chen, Carbon nanotube-polymer nanocomposite infrared sensor, Nano letters 8 (2008) 1142–1146.

[3] S. Cataldo, P. Salice, E. Menna, B. Pignataro, Carbon nanotubes and organic solar cells, Energy Environ. Sci. 5 (2012) 5919–5940.

[4] L. Vigderman, B.P. Khanal, E.R. Zubarev, Functional gold nanorods: synthesis, self-assembly, and sensing applications, Advanced materials (Deerfield Beach, Fla.) 24 (2012) 4811-41, 5014.

[5] G.R. Patzke, F. Krumeich, R. Nesper, Oxidic Nanotubes and Nanorods—Anisotropic Modules for a Future Nanotechnology, Angew. Chem. Int. Ed. 41 (2002) 2446–2461.

[6] J. Sapkota, M. Jorfi, C. Weder, E.J. Foster, Reinforcing Poly(ethylene) with Cellulose Nanocrystals, Macromolecular rapid communications (2014).

[7] J. Sapkota, S. Kumar, C. Weder, E.J. Foster, Influence of Processing Conditions on Properties of Poly (Vinyl acetate)/Cellulose Nanocrystal Nanocomposites, Macromol. Mater. Eng. 300 (2015) 562–571.

[8] J.-W. Liu, H.-W. Liang, S.-H. Yu, Macroscopic-scale assembled nanowire thin films and their functionalities, Chemical reviews 112 (2012) 4770–4799.

[9] K. Ariga, J.P. Hill, M.V. Lee, A. Vinu, R. Charvet, S. Acharya, Challenges and breakthroughs in recent research on self-assembly, Science and technology of advanced materials 9 (2008) 14109.

[10] G.M. Whitesides, B. Grzybowski, Self-assembly at all scales, Science (New York, N.Y.) 295 (2002) 2418–2421.

[11] R.-C. Brachvogel, F. Hampel, M. von Delius, Self-assembly of dynamic orthoester cryptates, Nature communications 6 (2015) 7129.

[12] P.A. Korevaar, C. Grenier, A.J. Markvoort, A.P.H.J. Schenning, T.F.A. de Greef, E.W. Meijer, Model-driven optimization of multicomponent self-assembly processes, Proceedings of the National Academy of Sciences of the United States of America 110 (2013) 17205–17210.

[13] H. Kar, S. Ghosh, Multicomponent gels: Remote control for self-assembly, Nature chemistry 7 (2015) 765–767.

[14] S. Whitelam, R. Schulman, L. Hedges, Self-assembly of multicomponent structures in and out of equilibrium, Physical review letters 109 (2012) 265506.

[15] Y. Li, O. Rios, J.K. Keum, J. Chen, M.R. Kessler, Photoresponsive Liquid Crystalline Epoxy Networks with Shape Memory Behavior and Dynamic Ester Bonds, ACS applied materials & interfaces 8 (2016) 15750–15757.

[16] S.-H. Hwang, Y.-B. Park, K. Han, D. Suk, Smart Materials and Structures Based on Carbon Nanotube Composites.

[17] M. de Voider, D. Reynaerts, C. van Hoof, S. Tawfick, A.J. Hart, A temperature sensor from a self-assembled carbon nanotube microbridge 2369–2372.

[18] L. Adler-Abramovich, D. Aronov, P. Beker, M. Yevnin, S. Stempler, L. Buzhansky, G. Rosenman, E. Gazit, Self-assembled arrays of peptide nanotubes by vapour deposition, Nature nanotechnology 4 (2009) 849–854.

[19] J.I. Lee, S.H. Cho, S.-M. Park, J.K. Kim, J.K. Kim, J.-W. Yu, Y.C. Kim, T.P. Russell, Highly aligned ultrahigh density arrays of conducting polymer nanorods using block copolymer templates, Nano letters 8 (2008) 2315–2320.

[20] M.J.A. Hore, A.L. Frischknecht, R.J. Composto, Nanorod Assemblies in Polymer Films and Their Dispersion-Dependent Optical Properties, ACS Macro Lett. 1 (2012) 115–121.

[21] M.J.A. Hore, R.J. Composto, Nanorod self-assembly for tuning optical absorption, ACS nano 4 (2010) 6941–6949.

[22] G.M. Whitesides, B. Grzybowski, Self-assembly at all scales, Science (New York, N.Y.) 295 (2002) 2418–2421.

[23] W. Liang, S. He, J. Fang, Self-assembly of J-aggregate nanotubes and their applications for sensing dopamine, Langmuir the ACS journal of surfaces and colloids 30 (2014) 805–811.

[24] R. Shvartzman-Cohen, M. Florent, D. Goldfarb, I. Szleifer, R. Yerushalmi-Rozen, Aggregation and self-assembly of amphiphilic block copolymers in aqueous dispersions of carbon nanotubes, Langmuir the ACS journal of surfaces and colloids 24 (2008) 4625–4632.

[25] C. Lara, S. Handschin, R. Mezzenga, Towards lysozyme nanotube and 3D hybrid self-assembly, Nanoscale 5 (2013) 7197–7201.

[26] Y. Yan, J. Huang, B.Z. Tang, Kinetic trapping - a strategy for directing the self-assembly of unique functional nanostructures, Chemical communications (Cambridge, England) 52 (2016) 11870–11884.

[27] K. van Workum, J.F. Douglas, Symmetry, equivalence, and molecular self-assembly, Physical review. E, Statistical, nonlinear, and soft matter physics 73 (2006) 31502.

[28] R.F. Hariadi, B. Yurke, E. Winfree, Thermodynamics and kinetics of DNA nanotube polymerization from single-filament measurements, Chem. Sci. 6 (2015) 2252–2267.

[29] M. Sahimi, S. Arbabi, Mechanics of disordered solids. II. Percolation on elastic networks with bond-bending forces, Phys. Rev. B 47 (1993) 703–712.

[30] J. Sapkota, A. Shirole, E.J. Foster, J.C. Martinez Garcia, M. Lattuada, C. Weder, Polymer nanocomposites with nanorods having different length distributions, Polymer (2016).

[31] L.A. Hough, M.F. Islam, P.A. Janmey, A.G. Yodh, Viscoelasticity of single wall carbon nanotube suspensions, Physical review letters 93 (2004) 168102.

[32] K. Kang, J.K.G. Dhont, Structural arrest and texture dynamics in suspensions of charged colloidal rods, Soft Matter 9 (2013) 4401.

[33] E. Grelet, Hexagonal order in crystalline and columnar phases of hard rods, Physical review letters 100 (2008) 168301.

[34] Z. DOGIC, S. FRADEN, Ordered phases of filamentous viruses, Current Opinion in Colloid & Interface Science 11 (2006) 47–55.

[35] G.J. Vroege, D.M.E. Thies-Weesie, A.V. Petukhov, B.J. Lemaire, P. Davidson, Smectic Liquid-Crystalline Order in Suspensions of Highly Polydisperse Goethite Nanorods, Adv. Mater. 18 (2006) 2565–2568.

[36] N. Puech, C. Blanc, E. Grelet, C. Zamora-Ledezma, M. Maugey, C. Zakri, E. Anglaret, P. Poulin, Highly Ordered Carbon Nanotube Nematic Liquid Crystals, J. Phys. Chem. C 115 (2011) 3272–3278.

[37] C. Zamora-Ledezma, C. Blanc, M. Maugey, C. Zakri, P. Poulin, E. Anglaret, Anisotropic thin films of single-wall carbon nanotubes from aligned lyotropic nematic suspensions, Nano letters 8 (2008) 4103–4107.

[38] G. Ao, D. Nepal, M. Aono, V.A. Davis, Cholesteric and nematic liquid crystalline phase behavior of double-stranded DNA stabilized single-walled carbon nanotube dispersions, ACS nano 5 (2011) 1450–1458.

[39] W. Song, I.A. Kinloch, A.H. Windle, Nematic liquid crystallinity of multiwall carbon nanotubes, Science (New York, N.Y.) 302 (2003) 1363.

[40] C.B. Murray, C.R. Kagan, M.G. Bawendi, Synthesis and Characterization of Monodisperse Nanocrystals and Close-Packed Nanocrystal Assemblies, Annu. Rev. Mater. Sci. 30 (2000) 545–610.

[41] M.C. Hersam, Progress towards monodisperse single-walled carbon nanotubes, Nature nanotechnology 3 (2008) 387–394.

[42] S. Mann, Self-assembly and transformation of hybrid nano-objects and nanostructures under equilibrium and non-equilibrium conditions, Nature materials 8 (2009) 781–792.

[43] A. Hirai, O. Inui, F. Horii, M. Tsuji, Phase separation behavior in aqueous suspensions of bacterial cellulose nanocrystals prepared by sulfuric acid treatment, Langmuir the ACS journal of surfaces and colloids 25 (2009) 497–502.

[44] J. Araki, S. Kuga, Effect of Trace Electrolyte on Liquid Crystal Type of Cellulose Microcrystals, Langmuir 17 (2001) 4493–4496.

[45] S. Mueller, J. Sapkota, A. Nicharat, T. Zimmermann, P. Tingaut, C. Weder, E.J. Foster, Influence of the nanofiber dimensions on the properties of nanocellulose/poly(vinyl alcohol) aerogels, J. Appl. Polym. Sci. 132 (2015) n/a-n/a.

[46] D. Bandera, J. Sapkota, S. Josset, C. Weder, P. Tingaut, X. Gao, E.J. Foster, T. Zimmermann, Influence of mechanical treatments on the properties of cellulose nanofibers isolated from microcrystalline cellulose, Reactive and Functional Polymers 85 (2014) 134–141.

[47] X.M. Dong, T. Kimura, J.-F. Revol, D.G. Gray, Effects of Ionic Strength on the Isotropic−Chiral Nematic Phase Transition of Suspensions of Cellulose Crystallites, Langmuir 12 (1996) 2076–2082.

[48] G.A. Buxton, A.C. Balazs, Modeling Mixtures of Nanorods and Polymers 275–286.

[49] S. Chakraborty, C.K. Choudhury, S. Roy, Morphology and Dynamics of Carbon Nanotube in Polycarbonate Carbon Nanotube Composite from Dissipative Particle Dynamics Simulation, Macromolecules 46 (2013) 3631–3638.

[50] M.A. Horsch, Z. Zhang, S.C. Glotzer, Self-assembly of polymer-tethered nanorods, Physical review letters 95 (2005) 56105.

[51] M.A. Horsch, Z. Zhang, S.C. Glotzer, Self-assembly of end-tethered nanorods in a neat system and role of block fractions and aspect ratio, Soft Matter 6 (2010) 945.

[52] M. Ionita, Multiscale molecular modeling of SWCNTs/epoxy resin composites mechanical behaviour, Composites Part B: Engineering 43 (2012) 3491–3496.

[53] M.D. Vo, D.V. Papavassiliou, Effect of Sodium Dodecyl Sulfate Adsorption on the Behavior of Water inside Single Walled Carbon Nanotubes with Dissipative Particle Dynamics Simulation, Molecules (Basel, Switzerland) 21 (2016) 500.

[54] M.D. Vo, D.V. Papavassiliou, Physical adsorption of polyvinyl pyrrolidone on carbon nanotubes under shear studied with dissipative particle dynamics simulations, Carbon 100 (2016) 291–301.

[55] Y.-C. Wang, S.-P. Ju, H.-Z. Cheng, J.-M. Lu, H.-H. Wang, Modeling of Polyethylene and Functionalized CNT Composites: A Dissipative Particle Dynamics Study, J. Phys. Chem. C 114 (2010) 3376–3384.

[56] A. Chami Khazraji, S. Robert, Interaction Effects between Cellulose and Water in Nanocrystalline and Amorphous Regions: A Novel Approach Using Molecular Modeling, Journal of Nanomaterials 2013 (2013) 1–10.

[57] A. Chami Khazraji, S. Robert, Self-Assembly and Intermolecular Forces When Cellulose and Water Interact Using Molecular Modeling, Journal of Nanomaterials 2013 (2013) 1–12.

[58] L. He, L. Zhang, H. Liang, Mono- or bidisperse nanorods mixtures in diblock copolymers, Polymer 51 (2010) 3303–3314.

[59] M.J.A. Hore, M. Laradji, Prospects of nanorods as an emulsifying agent of immiscible blends, The Journal of chemical physics 128 (2008) 54901.

[60] A. Gooneie, S. Schuschnigg, C. Holzer, Dissipative particle dynamics models of orientation of weakly-interacting anisometric silicate particles in polymer melts under shear flow: comparison with the standard orientation models, Macromol. Theory Simul. 25 (2016) 287–302.

[61] A. Gooneie, S. Schuschnigg, C. Holzer, A Review of Multiscale Computational Methods in Polymeric Materials, Polymers 9 (2017) 16.

[62] A. Gooneie, J. Gonzalez-Gutierrez, C. Holzer, Atomistic Modelling of Confined Polypropylene Chains between Ferric Oxide Substrates at Melt Temperature, Polym. 8 (2016) 361.

[63] A. Gooneie, S. Schuschnigg, C. Holzer, Orientation of anisometric layered silicate particles in uncompatibilized and compatibilized polymer melts under shear flow: A dissipative particle dynamics study, Macromol. Theory Simul. 25 (2016) 85–98.

[64] B. Zhou, W. Luo, J. Yang, X. Duan, Y. Wen, H. Zhou, R. Chen, B. Shan, Simulation of dispersion and alignment of carbon nanotubes in polymer flow using dissipative particle dynamics, Computational Materials Science 126 (2017) 35–42.

[65] D.A. Fedosov, G.E. Karniadakis, B. Caswell, Steady shear rheometry of dissipative particle dynamics models of polymer fluids in reverse Poiseuille flow, J. Chem. Phys. 132 (2010) 144103.

[66] A. Gooneie, S. Schuschnigg, C. Holzer, Coupled Orientation and Stretching of Chains in Mesoscale Models of Polydisperse Linear Polymers in Startup of Steady Shear Flow Simulations, Macromol. Theory Simul. 25 (2016) 170–186.

[67] O. Liba, D. Kauzlarić, Z.R. Abrams, Y. Hanein, A. Greiner, J.G. Korvink, A dissipative particle dynamics model of carbon nanotubes, Molecular Simulation 34 (2008) 737–748.

[68] P. Nikunen, I. Vattulainen, M. Karttunen, Reptational dynamics in dissipative particle dynamics simulations of polymer melts, Phys. Rev. E: Stat., Nonlinear, Soft Matter Phys. 75 (2007) 36713.

[69] A. Dufresne, Nanocellulose: From Nature to High Performance Tailored Materials, De Gruyter, France, 2012.

[70] M. Roman, Toxicity of Cellulose Nanocrystals: A Review, Industrial Biotechnology 11 (2015) 25–33.

[71] J. Sapkota, J.C. Natterodt, A. Shirole, E.J. Foster, C. Weder, Fabrication and Properties of Polyethylene/Cellulose Nanocrystal Composites, Macromol. Mater. Eng. (2016).

[72] R.D. Groot, P.B. Warren, Dissipative particle dynamics: Bridging the gap between atomistic and mesoscopic simulation, J. Chem. Phys. 107 (1997) 4423–4435.

[73] A. Maiti, J. Wescott, P. Kung, Nanotube–polymer composites: Insights from Flory–Huggins theory and mesoscale simulations, Molecular Simulation 31 (2005) 143–149.

[74] K. Lee, H.J. Lim, S.J. Yang, Y.S. Kim, C.R. Park, Determination of solubility parameters of single-walled and double-walled carbon nanotubes using a finite-length model, RSC Adv. 3 (2013) 4814.

[75] P. Español, P. Warren, Statistical Mechanics of Dissipative Particle Dynamics, Europhys. Lett. 30 (1995) 191–196.

[76] LAMMPS, http://lammps.sandia.gov/, accessed 8 November 2016.

[77] VMD, http://www.ks.uiuc.edu/Research/vmd/, accessed 8 November 2016.

[78] A. Shirole, J. Sapkota, E.J. Foster, C. Weder, Shape Memory Composites Based on Electrospun Poly(vinyl alcohol) Fibers and a Thermoplastic Polyether Block Amide Elastomer, ACS applied materials & interfaces 8 (2016) 6701–6708.

[79] Y. Zhao, M. Byshkin, Y. Cong, T. Kawakatsu, L. Guadagno, A. de Nicola, N. Yu, G. Milano, B. Dong, Self-assembly of carbon nanotubes in polymer melts: simulation of structural and electrical behaviour by hybrid particle-field molecular dynamics, Nanoscale 8 (2016) 15538–15552.

[80] M. Wan, X. Li, L. Gao, W. Fang, Self-assembly of gold nanorods coated with phospholipids: a coarse-grained molecular dynamics study, Nanotechnology 27 (2016) 465704.

[81] S. Khani, S. Jamali, A. Boromand, M.J.A. Hore, J. Maia, Polymer-mediated nanorod self-assembly predicted by dissipative particle dynamics simulations, Soft Matter 11 (2015) 6881–6892.

[82] K. Thorkelsson, A.J. Mastroianni, P. Ercius, T. Xu, Direct nanorod assembly using block copolymer-based supramolecules, Nano letters 12 (2012) 498–504.

[83] C. Avendaño, F.A. Escobedo, Phase behavior of rounded hard-squares, Soft Matter 8 (2012) 4675.

[84] S. Gupta, Q. Zhang, T. Emrick, T.P. Russell, "Self-corralling" nanorods under an applied electric field, Nano letters 6 (2006) 2066–2069.

[85] A. Thess, R. Lee, P. Nikolaev, H. Dai, P. Petit, J. Robert, C. Xu, Y.H. Lee, S.G. Kim, A.G. Rinzler, D.T. Colbert, G.E. Scuseria, D. Tomanek, J.E. Fischer, R.E. Smalley, Crystalline Ropes of Metallic Carbon Nanotubes, Science 273 (1996) 483–487.

[86] M. Surve, V. Pryamitsyn, V. Ganesan, Dispersion and Percolation Transitions of Nanorods in Polymer Solutions, Macromolecules 40 (2007) 344–354.

[87] B. Pradhan, S.K. Srivastava, Synergistic effect of three-dimensional multi-walled carbon nanotube-graphene nanofiller in enhancing the mechanical and thermal properties of high-performance silicone rubber, Polym. Int. 63 (2014) 1219–1228.

[88] S.-Y. Yang, W.-N. Lin, Y.-L. Huang, H.-W. Tien, J.-Y. Wang, C.-C.M. Ma, S.-M. Li, Y.-S. Wang, Synergetic effects of graphene platelets and carbon nanotubes on the mechanical and thermal properties of epoxy composites, Carbon 49 (2011) 793–803.

[89] Y. Wang, H. Tian, L. Zhang, Role of starch nanocrystals and cellulose whiskers in synergistic reinforcement of waterborne polyurethane, Carbohydrate Polymers 80 (2010) 665–671.

[90] J. Li, P.C. Ma, W.S. Chow, C.K. To, B.Z. Tang, J.-K. Kim, Correlations between Percolation Threshold, Dispersion State, and Aspect Ratio of Carbon Nanotubes, Adv. Funct. Mater. 17 (2007) 3207–3215.

[91] B. Nikoobakht, Z.L. Wang, M.A. El-Sayed, Self-Assembly of Gold Nanorods, J. Phys. Chem. B 104 (2000) 8635–8640.

[92] F. Jativa, C. Schutz, L. Bergstrom, X. Zhang, B. Wicklein, Confined self-assembly of cellulose nanocrystals in a shrinking droplet, Soft Matter 11 (2015) 5374–5380.

[93] A.G. Dumanli, G. Kamita, J. Landman, H. van der Kooij, B.J. Glover, J.J. Baumberg, U. Steiner, S. Vignolini, Controlled, Bio-inspired Self-Assembly of Cellulose-Based Chiral Reflectors, Advanced optical materials 2 (2014) 646–650.

[94] K. Thorkelsson, J.H. Nelson, A.P. Alivisatos, T. Xu, End-to-end alignment of nanorods in thin films, Nano letters 13 (2013) 4908–4913.

[95] X. Zeng, X. Xu, P.M. Shenai, E. Kovalev, C. Baudot, N. Mathews, Y. Zhao, Characteristics of the Electrical Percolation in Carbon Nanotubes/Polymer Nanocomposites, J. Phys. Chem. C 115 (2011) 21685–21690.

[96] A.A. Vasileiou, M. Kontopoulou, H. Gui, A. Docoslis, Correlation between the length reduction of carbon nanotubes and the electrical percolation threshold of melt

compounded polyolefin composites, ACS applied materials & interfaces 7 (2015) 1624–1631.